MIS Slow-Wave Structures Over a Wide Range of Parameters

James P. K. Gilb, *Student Member, IEEE,* and Constantine A. Balanis, *Fellow, IEEE*

Abstract—**The high dielectric losses of the semiconducting substrates used in MMIC's and VLSI interconnects can strongly affect all of the characteristics of these lines. No single approximate formulation is accurate over a wide range of substrate parameters or over a large frequency range; thus it is necessary to use a full-wave approach. Multi-conductor MIS structures are analyzed with the spectral domain approach over a wide range of frequency and substrate loss. The modal attenuation and propagation constants are presented for two and four conductor structures as a function of the substrate loss tangent. Single conductor structures are characterized with contour plots showing the complex effective dielectric constant as a function of both frequency and conductivity. MIS slow-wave structures are analyzed for both Si–SiO_2 and GaAs configurations.**

I. Introduction

SINCE the substrates used in most MIC's have small loss tangents, dielectric losses usually play a secondary role in the attenuation and distortion of signals. However, the semiconducting substrates used in MMIC's and VLSI interconnects cause dielectric losses to become a major contributor to signal attenuation. In addition, high dielectric losses can cause a significant change in the phase constant, as is the case with slow-wave structures. Since the loss in these structures is not small, i.e. $\tan\delta \not\ll 1$, perturbational and approximate formulas do not give accurate results and a full wave approach must be used.

For slow-wave structures, those with moderate conductivities at lower frequencies, the propagation constant and attenuation constant have been obtained using a parallel plate waveguide approximation [1], [2] which gives good results only for very wide center conductors. For very high conductivities or very high frequencies, the transmission line is operating in the skin effect region and the attenuation constant can be computed using the incremental inductance rule [3].

However, if the conductivity is constant with frequency, then no single approximate formulation is accurate over the wide range of frequencies necessary to characterize pulse distortion. In addition, none of the approximations is appropriate in the transition regions mentioned in [2]. Thus a full-wave approach is necessary for accurate characterization of dielectric losses in structures with semiconducting substrates. Mode-matching has also been applied to give accurate results for a limited range of substrate parameters [4], [5]. The spectral domain approach (SDA) with complex permittivities for the dielectric layers is also used to analyze these structures. The SDA is easy to formulate for multi-layer, multi-conductor structures, it gives quick and accurate results, and it can be used for all conductivities and frequencies. The SDA has been used to characterize Coplanar Waveguide (CPW) [4], single and coupled microstrips on a single substrate [6], [7] and for multiple microstrips on multi-layer, lossy substrates [8]. Although single-conductor, multi-layer, lossy microstrip structures have received some attention, there are still many important characteristics of these structures which have not yet been addressed. In addition, multi-conductor structures, such as those found in high-speed, high-density digital interconnects, have received very little attention. Also of interest is the behavior of the modal attenuation constants for multi-conductor microstrips in the low-loss, slow-wave, and skin-effect regions as a function of the substrate parameters.

This paper studies lossy multi-layer, multi-conductor microstrip structures using the SDA. The modal attenuation and propagation constants of lossy, multi-layer, multi-conductor structures are given over a wide range of substrate parameters and frequencies, covering all three regions; low loss, slow wave, and skin effect. The combinations of frequency and dielectric loss that give either the maximum or minimum dielectric loss coefficient are computed, showing how they are related to the extrema of the derivative of the real part of the effective dielectric constant. Both Si–SiO_2 and GaAs configurations of MIS slow-wave structures are analyzed as a function of the substrate loss and frequency.

II. Full Wave Analysis

The SDA has been discussed extensively in previous works; therefore the technical details are omitted here. A very good explanation of the method can be found in [9] and an excellent list of references is given in [10]. The Green's function for structures with multiple substrates and/or superstrates can be computed using a simple re-

Manuscript received March 31, 1992; revised August 3, 1992. This work was partially supported by the U.S. Army Research Office under grant DAAL03-92-G-0262.

The authors are with the Department of Electrical Engineering Telecommunications Research Center, Arizona State University, Tempe, Arizona 85287-7206.

IEEE Log Number 9203692.

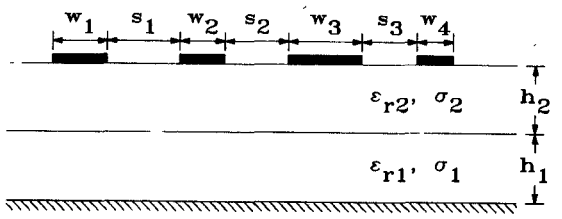

Fig. 1. Geometry of an asymmetric multi-layer, multi-conductor interconnect.

cursive formulation [11]. The geometry for multi-layer, multi-conductor interconnects is shown in Fig. 1. Two substrates are shown in the figure, although any finite number of substrates or superstrates can be easily considered using the recurrence formulation from [11]. The center conductor is assumed to be infinitely thin and perfectly conducting. Although including the effect of the ohmic losses and finite center conductor thickness is important in many applications, it is beyond the scope of the current research.

For a conductor centered at $x = x_i$ with a width $w = w_i$, the current density expansion functions used in this paper are given by:

$$J^i_{zn}(x) = a^i_n \frac{T_n[2(x - x_i)/w_i]}{\sqrt{1 - [2(x - x_i)/w_i]^2}} \tag{1}$$

$$J^i_{xn}(x) = -jb^i_n \frac{w_i}{2} U_{n-1}[2(x - x_i)/w_i] \cdot \sqrt{1 - [2(x - x_i)/w_i]^2} \tag{2}$$

for $n = 0, 1, 2, \cdots$, and $|x - x_i| \leq w_i/2$. $T_n(x)$ and $U_n(x)$ are the Chebyshev polynomials of the first and second kind, respectively, as given in [12]. Results obtained with this method have been compared and agree very closely with results presented in the literature [7], [8].

To consider lossy structures with the SDA, a complex permittivity is defined for the ith dielectric layer as

$$\epsilon^*_i = \epsilon'_i - j\epsilon''_i = \epsilon'_i - j\frac{\sigma_i}{\omega} \tag{3}$$

and

$$\tan \delta_i = \frac{\epsilon''_i}{\epsilon'_i} = \frac{\sigma_i}{\epsilon'_i \omega}. \tag{4}$$

When Galerkin's method is applied to the dyadic Green's functions, which are now complex because of the complex permittivity, it leads to two equations (the real and imaginary parts of the determinant) with two unknowns (the real, α_z, and imaginary, β_z, parts of the complex propagation constant, γ_z). The complex propagation constant is then obtained by using a non-linear root finder to search for the zero of the determinant of the impedance matrix [11].

For a "good" dielectric, it is usually assumed that the loss tangent is constant with frequency. For semiconductors or conductors, on the other hand, it is usually assumed that the conductivity or resistivity is constant with frequency. Since accurate measurements of the dielectric constant versus frequency are not readily available for most materials, one of the two assumptions, either constant tan δ or constant σ, will be used in this paper. In either case, it will be made clear which assumption is used.

III. Approximate Analysis

Many of the characteristics of lossy, multi-layer structures are more easily explained by analyzing a simpler structure, the parallel plate waveguide. This model is a limiting case for very wide microstrips and behaves in a manner similar to that of the general microstrip structure. In [2], a two-layer parallel plate structure is studied where only one layer is lossy, as shown in Fig. 2. The behavior of this structure as a function of frequency and dielectric loss can be divided up into three main regions: 1) low-loss region, 2) slow-wave region, and 3) skin-effect region. In the low-loss region, the losses in the substrate do not significantly affect the phase constant and so the structure can be analyzed by using a perturbational approach with the lossless case.

For moderate dielectric losses and relatively low frequencies the structure is in the slow-wave region, so named because of the significant decrease in the phase velocity of the structure. Unlike the lossless microstrip case, ϵ'_{reff} in the slow wave region can be much larger than the relative dielectric constants of any of the substrate layers. For the two substrate case, the upper limit of ϵ'_{reff}, which is achieved for very wide center conductors, is given by the static value of the Maxwell–Wagner permittivity [13], $\epsilon'_{rs} = \epsilon_{r2}(h_1 + h_2)/h_2$. In the slow-wave region, the dielectric loss coefficient, α_d, decreases linearly with increasing tan δ_1 or σ_1, reaches a minimum point, and then begins to increase linearly again. The minimum point can be predicted using the parallel plate waveguide approximation [2] and occurs for a conductivity of

$$\sigma_{1\min} = \sqrt{\frac{3\epsilon_0\epsilon_{r2}}{\mu_0\mu_{r2}h_1h_2}} \tag{5}$$

or for a loss tangent of

$$\tan \delta_{1\min} = \frac{c}{\omega\epsilon_{r1}}\sqrt{\frac{3\epsilon_{r2}}{\mu_{r2}h_1h_2}}. \tag{6}$$

If either the dielectric loss or the frequency is very high, the structure is said to be in the skin-effect region. In this region, the fields only penetrate a small distance into the lower substrate. With increasing frequency or dielectric loss, the dielectric loss coefficient tends to decrease as more of the fields are contained in the lossless, upper substrate rather than in the lossy, lower substrate. In this region, the lower substrate behaves like a conductor with finite loss. The dielectric loss coefficient, or alternately the conduction loss coefficient, should decrease in proportion to $1/\sqrt{\sigma_1}$ in the skin effect region.

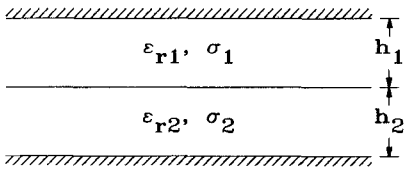

Fig. 2. Geometry of a two-layer parallel plate waveguide.

Connecting the low-loss and slow-wave regions and slow-wave and skin-effect regions are the transition regions where ϵ'_{reff} is changing rapidly and ϵ''_{reff} achieves its maximum value. The transition from low-loss to slow-wave for the parallel plate waveguide structure can be described using the following approximations [2]

$$\epsilon'_{reff} = \epsilon_{r\infty} + \frac{\epsilon_{rs} - \epsilon_{r\infty}}{1 + k^2\omega^2/\sigma_1^2} \tag{7}$$

$$\epsilon''_{reff} = \frac{(\epsilon_{rs} - \epsilon_{r\infty})k\omega/\sigma_1}{1 + k^2\omega^2/\sigma_1^2} \tag{8}$$

where

$$\epsilon_{r\infty} = \frac{h_1 + h_2}{h_1/\epsilon_{r1} + h_2/\epsilon_{r2}} \tag{9}$$

$$k = \epsilon_0 h_1(\epsilon_{r1}/h_1 + \epsilon_{r2}/h_2). \tag{10}$$

The minima of ϵ''_{reff} occur at the end points of the interval $0 \le \sigma_1 < \infty$, i.e. when the substrate is lossless, $\sigma_1 = 0$, and when it is a perfect conductor, $\sigma_1 \to \infty$. The maximum ϵ''_{reff} occurs for $\sigma_1 = k\omega$ or when $\tan\delta_1 = k/(\epsilon_0\epsilon_{r1})$.

In the transition regions, ϵ'_{reff} is changing rapidly and so we are interested in the behavior of its derivative with respect to the dielectric loss. The minima of $\partial\epsilon'_{reff}/\partial\sigma_1$ occur at the endpoints of the interval $0 \le \sigma_1 < \infty$, which coincides with the minima of ϵ'_{reff}. The maximum of the first derivative, however, does not coincide with the maximum value of ϵ''_{reff}, instead it occurs for $\sigma_1 = k\omega/\sqrt{3}$ or when $\tan\delta_1 = k/(\epsilon_0\epsilon_{r1}\sqrt{3})$. On the other hand, when $\partial\epsilon'_{reff}/\partial(\ln\sigma_1)$ is computed, the maximum occurs for $\sigma_1 = k\omega$ or when $\tan\delta_1 = k/(\epsilon_0\epsilon_{r1})$, which is the same as the maximum of ϵ''_{reff}.

In the transition from the slow-wave region to the skin-effect region, the complex ϵ_{reff} can be given approximately as [2]

$$\epsilon^*_{reff} = \epsilon_{r2}\frac{h_1 + h_2}{h_2}\left[1 - \frac{h_1}{h_1 + h_2}\left(1 - \frac{\tanh(\gamma_{y1}h_1)}{\gamma_{y1}h_1}\right)\right] \tag{11}$$

where

$$\gamma_{y1}h_1 = (1 + j)\sqrt{f\sigma_1\pi\mu_0 h_1^2}. \tag{12}$$

In (11) μ_{reff} and ϵ_{reff} from [2] have been combined since it is not possible to distinguish between the two parameters in a full-wave analysis. Setting the real and imaginary parts of the derivatives of (11) to zero results in complicated transcendental equations which do not have closed form solutions. Solving these equations numerically gives the following values of the frequency-conductivity product;

$$\text{maximum } \epsilon''_{reff} \to f\sigma_1 = 1.27/(\pi\mu_0 h_1^2) \tag{13}$$

$$\text{maximum } \frac{\partial\epsilon'_{reff}}{\partial\sigma_1} \to f\sigma_1 = 0.71/(\pi\mu_0 h_1^2) \tag{14}$$

$$\text{maximum } \frac{\partial\epsilon'_{reff}}{\partial(\ln\sigma_1)} \to f\sigma_1 = 1.24/(\pi\mu_0 h_1^2) \tag{15}$$

In this region, the maximum ϵ''_{reff} and maximum $\partial\epsilon'_{reff}/\partial(\ln\sigma_1)$ are close to each other, but are not exactly equal as are the maxima in the low-loss to slow-wave transition region.

IV. Results

Fig. 3 shows ϵ_{reff} and α_d for single and coupled microstrips on two substrates as a function of the loss tangent of the lowest substrate computed using the lossy SDA approach. Since the frequency is held constant at 1 GHz, varying the loss tangent is equivalent to varying the conductivity (for this configuration, $\sigma_1(\Omega\text{m})^{-1} = 0.540\tan\delta_1$). For $\tan\delta_1 << 1$, the structure is in the low-loss region and α_d increases linearly with increasing $\tan\delta_1$, as expected. In this region, the lower substrate has the characteristics of a "good" dielectric. When $\tan\delta_1$ is very large, α_d decreases with a slope of $-\frac{1}{2}$ on the log-log scale, indicating a $1/\sqrt{\tan\delta_1}$ behavior. This is consistent with the skin effect which has a $1/\sqrt{\sigma_1}$ behavior for the loss coefficient. In this region, the lower substrate has the characteristics of a "good" conductor. In the slow-wave region, the dielectric attenuation constant decreases linearly until it reaches a minimum and then begins to increase linearly. Using (5) to predict the minimum attenuation gives $\tan\delta_{1\,\min} = 102$, which is close to the location of the actual minimum. The largest values of α_d occur in the middle of the transitions from low-loss to slow-wave regions and from slow-wave to skin effect regions.

Within each of the three regions (low-loss, slow-wave, and skin-effect) ϵ'_{reff} is relatively constant with changing loss tangent. In the low-loss region, the ϵ'_{reff}'s for both modes and the isolated case are approximately the same as the corresponding values of ϵ'_{reff} of the lossless, two-substrate structure. For each of the three cases, in the skin-effect region, ϵ'_{reff} is larger than in the low-loss region since the lower substrate acts as a lossy ground plane, thereby reducing the height that the center conductor is above the ground plane. In the slow-wave region, ϵ'_{reff} for both modes and the isolated case rise to large values, as expected. The even mode ϵ'_{reff} increases to a higher value than that of the odd mode since the fields of the even mode are concentrated more in the lower substrate. The odd mode, on the other hand, has most of its fields concentrated in the air and in the lossless, upper substrate. Thus, changes in the dielectric loss do not affect the odd mode as much as they do the even mode.

Since ϵ^*_{reff} is an analytic function it is possible to relate the real and imaginary parts via the Kramers–Kronig re-

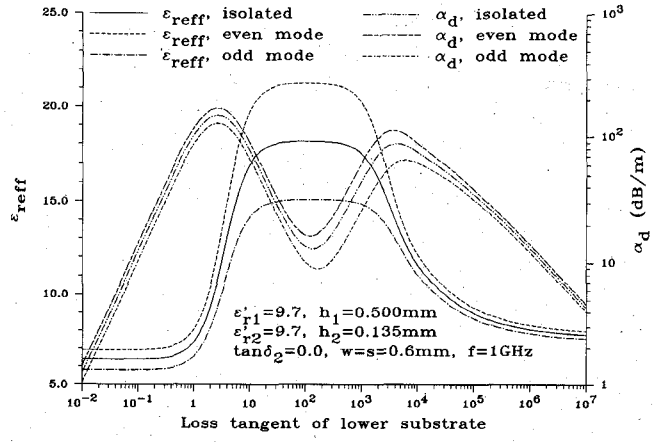

Fig. 3. ϵ'_{reff} and α_d for single and coupled microstrips as a function of the loss tangent of the lower substrate at a frequency of 1 GHz.

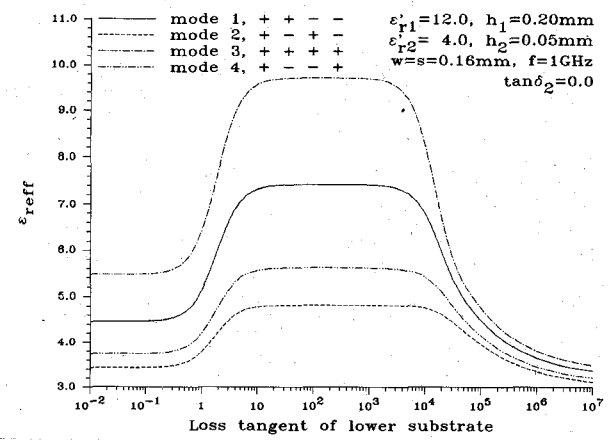

Fig. 4. ϵ'_{reff} of four symmetric coupled microstrips as a function of the loss tangent of the lower substrate, tan δ_1, at a frequency of 1 GHz.

lations [14], [15]. Thus the behavior of ϵ^*_{reff} as a function of tan δ_1 is similar to the behavior of ϵ^*_r as a function of frequency. The connection between the real and imaginary parts of ϵ^*_{reff} is discussed in more detail later in the paper.

A four line, symmetric microstrip structure on an Si–SiO_2 substrate is analyzed in Fig. 4 and Fig. 5 as a function of the loss tangent of the lower substrate, the Si layer, at a frequency of 1 GHz. The ϵ_{reff}'s of the four independent modes are given in Fig. 4 with the corresponding α_d's presented in Fig. 5. The plus and minus signs next to the mode numbers refer to the relative magnitudes of the currents on each of the conductors for that mode. The slowest mode, mode 3, has even/even symmetry which concentrates most of the fields in the substrates. Thus the ϵ_{reff} for this mode is affected the most by changes in the conductivity of the Si layer. The fastest mode, mode 2, however, has odd/odd symmetry and so the electric fields for this mode are concentrated more in the air and upper substrate. Thus the ϵ'_{reff} of mode 2 changes much less than that of mode 3 with changes in the conductivity of the Si layer.

The dielectric loss coefficient is plotted in Fig. 5 for the four modes versus the loss tangent of the Si substrate. As with the symmetric coupled microstrip structure, the modal attenuation coefficients increase linearly in the low-loss region and decrease with a $1/\sqrt{\tan \delta_1}$ dependence in the skin effect region. Also, the attenuation coefficients of each of the four modes reach a minimum in the slow-wave region for loss tangents between 100 and 300. The predicted minimum for a single strip on this substrate using (6) is 138. As with the ϵ'_{reff}, the variations of α_d for the modes can be related to the symmetry of the modes. Mode 3, which has the most electric field concentrated in the lower substrate, has higher losses and enters the skin effect region sooner than the other modes. Mode 2, on the other hand, has its electric field concentrated in the air and so it has the lowest losses and enters the skin effect region last.

To illustrate how frequency and dielectric losses affect the complex ϵ^*_{reff}, contour plots of ϵ'_{reff} and $\log_{10}(\epsilon''_{reff})$ are

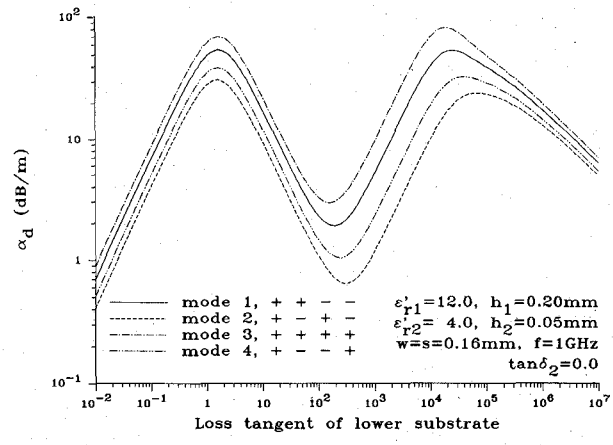

Fig. 5. α_d of four symmetric coupled microstrips as a function of the loss tangent of the lower substrate, tan δ_1, at a frequency of 1 GHz, with the same dimensions as in Fig. 4.

presented in Figs. 6–9. Figs. 6 and 8 were computed assuming that tan δ_1 is constant with frequency, while Figs. 7 and 9 used the assumption of constant conductivity with frequency. Figs. 6 and 7 show the value of ϵ'_{reff} while Figs. 8 and 9 give the value of $\log_{10}(\epsilon''_{reff})$.

In Figs. 6 and 7, the large open space in the lower, center part of the contour plots is the slow-wave region. In this area, ϵ'_{reff} is a maximum and changes very little with either frequency or dielectric loss, maintaining a value of around 26.5. The low-loss region is located on the left side of Fig. 6 and in the upper left of Fig. 7. In Fig. 6, ϵ'_{reff} is constant for low frequencies and then begins to increase slowly around 30 GHz because of the dispersive properties of the structure. For the constant conductivity assumption, Fig. 7, ϵ'_{reff} decreases rapidly from its slow-wave value, approaching the low-loss, quasi-static value. It then begins to increase with increasing frequency, again due to dispersion. The skin effect region is in the upper right of the contour plots. The transition for the slow-wave value of ϵ'_{reff} to its skin-effect value is fairly rapid. The value of ϵ'_{reff} in the skin-effect region ($\epsilon'_{reff} \simeq 3.7$) is lower than that of the low-loss region ($\epsilon'_{reff} \simeq 6.1$) because the low-loss region is a two-substrate structure

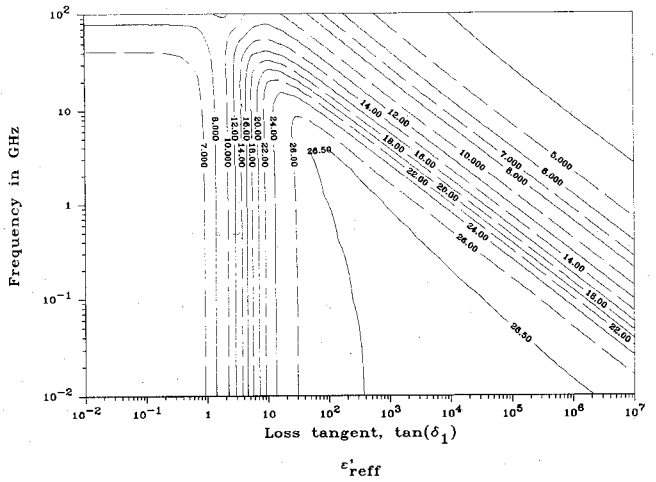

Fig. 6. Contour plot of ϵ'_{reff} as a function of the frequency and the loss tangent of the lower substrate, tan δ_1 (h_1 = 0.24 mm, h_2 = 0.01 mm, ϵ_{r1} = 12, ϵ_{r2} = 4.0, tan δ_2 = 0, w = 0.16 mm).

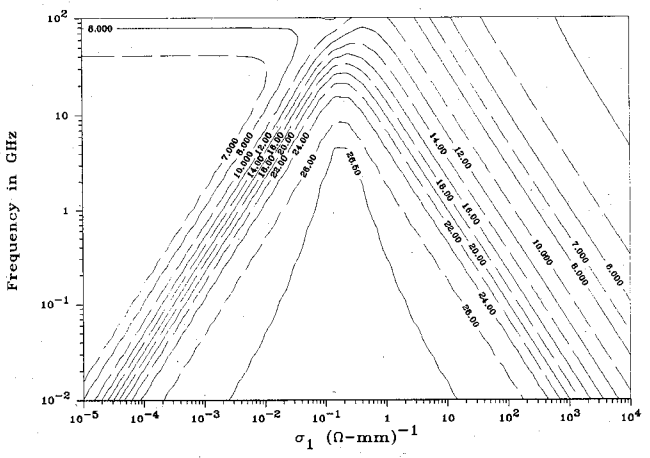

Fig. 7. Contour plot of ϵ'_{reff} as a function of the frequency and the conductivity of the lower substrate, σ_1, with the same dimensions as in Fig. 6.

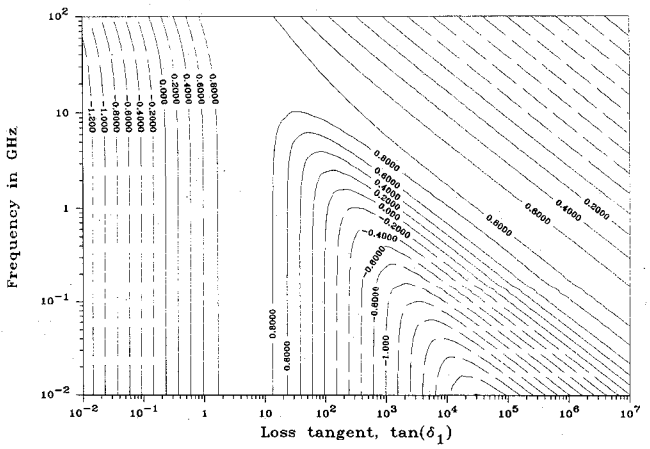

Fig. 8. Contour plot of $\log_{10}(\epsilon''_{reff})$ as a function of the frequency and the loss tangent of the lower substrate, tan δ_1, with the same dimensions as in Fig. 6.

dominated by the Si layer (ϵ_r = 12) while in the skin-effect region it is essentially a one-substrate structure of SiO_2 (ϵ_r = 4.0).

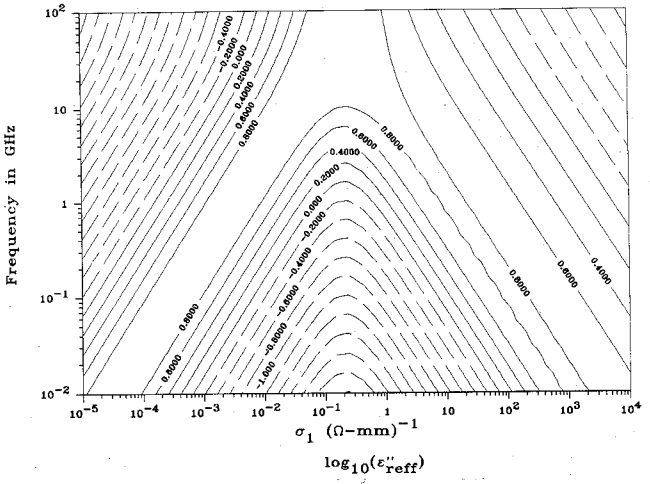

Fig. 9. Contour plot of $\log_{10}(\epsilon''_{reff})$ as a function of the frequency and the conductivity of the lower substrate, σ_1, with the same dimensions as in Fig. 6.

In Figs. 8 and 9 the logarithm of ϵ''_{reff} is plotted since ϵ''_{reff} varies over a very wide range of values with changing frequency and dielectric loss. The slow-wave, low-loss, and skin-effect regions in Figs. 8 and 9 are located in the same areas as in Figs. 6 and 7, respectively. One difference in the behavior of the real and imaginary parts of ϵ^*_{reff} is that within each of the three regions, the value of ϵ'_{reff} is relatively constant with changing frequency and dielectric loss, while the value of ϵ''_{reff} is always changing within the regions. The only exception to this occurs in the low-loss region of Fig. 8 where the value of ϵ''_{reff} is relatively constant with respect to frequency when tan δ_1 is constant with frequency. Another point to note is that when ϵ'_{reff} is a maximum (in the center of the slow-wave region), ϵ''_{reff}, and hence the dielectric losses, are at a minimum. Using (5), the value of σ_1 which gives minimum dielectric loss is $\sigma_{1\,min} = 0.092\,(\Omega\ mm)^{-1}$, which is close to actual value for this structure.

While the maximum ϵ'_{reff} occurs when ϵ''_{reff} is at a minimum, the location of the maximum ϵ''_{reff} does not occur with minimum ϵ'_{reff}. Instead, ϵ''_{reff} is greatest in the transition regions when ϵ'_{reff} is changing most rapidly, i.e. when the derivative of ϵ'_{reff} with respect to either frequency or the dielectric loss parameter is greatest, just as in case of the parallel plate waveguide. In Fig. 10, the maximum ϵ''_{reff}, and maximum of the partial derivatives of ϵ'_{reff} computed with the SDA are plotted for the same structure in Fig. 7 over the same range of conductivity and frequency. Also included are the curves representing the maximum ϵ''_{reff}, and the maximum of the partial derivatives of ϵ'_{reff} computed using the parallel plate waveguide model. The maxima predicted by the parallel plate waveguide model are shifted slightly to the right in the transition from low-loss to slow-wave and in the opposite direction in the transition from slow-wave to skin-effect. This shift occurs because the parallel plate waveguide model is only valid for very wide strips, whereas the width used for the full-wave analysis is relatively small.

Since the transitions are shifted in toward the slow-wave

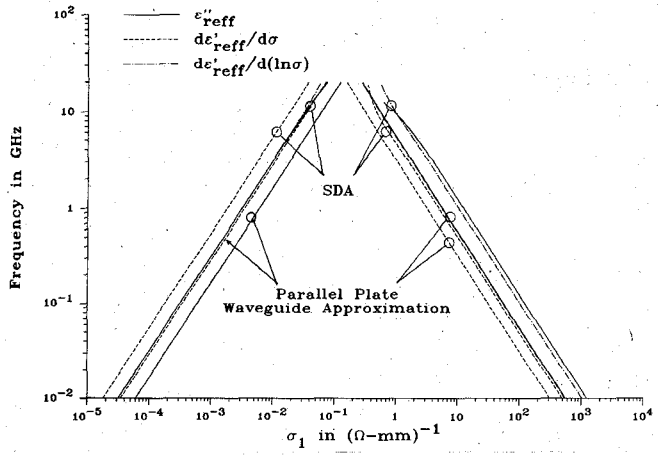

Fig. 10. Maximum ϵ''_{reff}, $\partial\epsilon'_{reff}/\partial\sigma$, and $\partial\epsilon'_{reff}/\partial(\ln\sigma)$ computed using the SDA and the parallel plate waveguide approximation as a function of the frequency and conductivity of the lower substrate, σ_1, with the same dimensions as in Fig. 6.

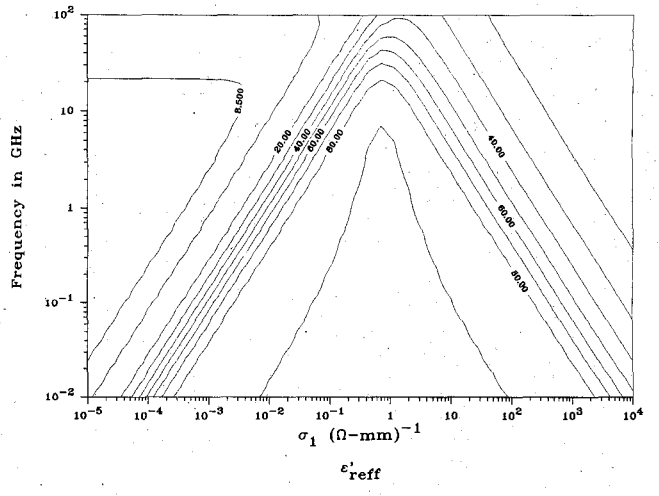

Fig. 11. Contour plot of ϵ'_{reff} as a function of frequency and the conductivity of the lower substrate, σ_1, for a GaAs slow-wave structure ($h_1 = 100$ μm, $h_2 = 5$ μm, $\epsilon_{r1} = \epsilon_{r2} = 12.9$, $\tan\delta_2 = 0.0004$, $w = 100$ μm).

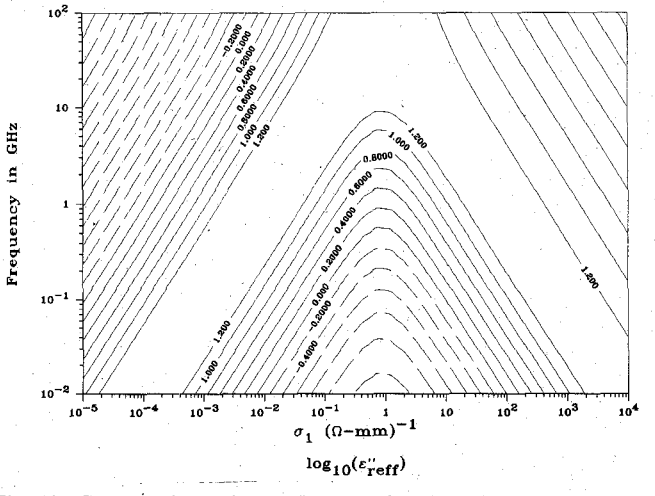

Fig. 12. Contour plot of $\log_{10}(\epsilon''_{reff})$ as a function of frequency and the conductivity of the lower substrate, σ_1, for a GaAs slow-wave structure with the same dimensions as in Fig. 11.

region in Fig. 10, the parallel plate waveguide model predicts a slightly smaller slow-wave region than is computed using the SDA. The SDA predicts a larger slow-wave region because it uses a smaller center conductor width. The smaller center conductor width causes more of the fields to be contained in the air and in the upper substrate which are lossless, than in the lossy lower substrate, reducing the value of ϵ'_{reff} that is achieved in the slow-wave region. Thus, a structure with a smaller center conductor width enters the slow-wave region earlier and transitions to the skin effect region later since it needs to reach a smaller value of ϵ'_{reff}. This behavior is also observed in the odd mode in Fig. 3 or in mode 2 in Fig. 4. This has the effect of increasing the size of the slow-wave region as the width of the center conductor decreases.

The maxima obtained using the SDA show behavior that closely parallels the results of the parallel plate waveguide model in the transition region from low-loss to skin-effect. Using the full-wave approach, the ratio of the conductivities which give maximum ϵ''_{reff} and the maximum $\partial\epsilon'_{reff}/\partial\sigma_1$ is approximately 1.73, i.e. a constant offset of $\log_{10}(\sigma_1) = 0.239$. This is in close agreement with the results of the parallel plate waveguide model which predicts the ratio of the maxima of $\partial\epsilon'_{reff}/\partial\sigma_1$ and ϵ''_{reff} to be $\sqrt{3} = 1.7321$. Likewise, the parallel plate waveguide model predicts that the maximum of ϵ''_{reff} will correspond to the maximum of $\partial\epsilon'_{reff}/\partial(\ln\sigma_1)$ and the results from the SDA also show this behavior. In fact, in Fig. 10 it is not possible to distinguish between the graphs of the maxima of ϵ''_{reff} and the maxima of $\partial\epsilon'_{reff}/\partial(\ln\sigma_1)$ for either of the two methods.

In the transition region from slow-wave to skin-effect, the agreement between the parallel plate waveguide model and the SDA is not as good. From the parallel plate waveguide model, the ratio of the maxima of ϵ''_{reff}, (13), to the maxima of $\partial\epsilon'_{reff}/\partial(\ln\sigma_1)$, (15), is 1.023, while the same ratio using the SDA is about 1.17. Likewise, the ratio of the maxima of ϵ''_{reff} to the maxima of $\partial\epsilon'_{reff}/\partial\sigma_1$ is predicted to be 1.78 using the parallel plate waveguide and it is about 2.2 using the SDA. These discrepancies are most likely due to the approximations that were made in arriving at (11).

MIS slow-wave structures can also be constructed using a thin layer of semi-insulating GaAs on a doped GaAs substrate. The real and imaginary parts of the complex effective dielectric constant for this structure are shown as contour plots in Figs. 11 and 12 as a function of frequency and the conductivity of the doped GaAs. A 100 μm layer of doped GaAs is used for the lower substrate with a 5 μm layer of semi-insulating GaAs for the upper substrate and a 100 μm center conductor width. A conductivity of $10^{-3}(\Omega\text{ mm})^{-1}$ corresponds to p-GaAs doped at 10^{14} cm^{-3} and a conductivity of $10^{4}(\Omega\text{ mm})^{-1}$ to n-GaAs doped at 10^{20} cm^{-3}. The upper substrate is very thin and so ϵ'_{reff} is very large in the slow-wave region, around 89. Since the real part of the relative dielectric constants of the substrates are the same, the ϵ'_{reff} in the low-loss region is lower than in the skin-effect region as

in Fig. 3. The imaginary part of ϵ^*_{reff}, in Fig. 12, shows the same general behavior as the Si-SiO_2 structure.

V. Conclusion

The presence of high dielectric losses or a conductivity that is constant with frequency requires the use of a full-wave analysis. The SDA was used to accurately analyze multi-layer, multi-conductor structures over a wide range of frequency and substrate loss. Results for single, two, and four conductor structures were presented which show how the substrate dielectric loss affects both the real and imaginary parts of the effective dielectric constant. MIS slow-wave structures were analyzed using both Si-SiO_2 and GaAs configurations. Contour plots of the complex effective dielectric constant showed the locations and characteristics of three regions of operation, slow-wave, low-loss, and skin-effect. The maximum and minimum ϵ''_{reff} were computed with the SDA as a function of frequency and conductivity showing how they are related to the extrema of the derivative of ϵ'_{reff}.

Acknowledgment

The authors would like to thank Dr. J. W. Mink of the Electronics Division, Army Research Office, for his interest and support of the project.

References

[1] H. Guckel, P. A. Brennan, and I. Palócz, "A parallel-plate waveguide approach to microminiaturized, planar transmission lines for integrated circuits," *IEEE Trans. Microwave Theory Tech.*, vol. MTT-15, pp. 468–476, Aug. 1967.

[2] H. Hasegawa, M. Furukawa, and H. Yanai, "Properties of microstrip line on Si-SiO_2 system," *IEEE Trans. Microwave Theory Tech.*, vol. MTT-19, pp. 869–881, Nov. 1971.

[3] H. A. Wheeler, "Formulas for skin effect," *Proc. IRE*, vol. 30, pp. 412–424, Sept. 1942.

[4] Y. Fukuoka, Y.-C. Shih, and T. Itoh, "Analysis of slow-wave coplanar waveguide for monolithic integrated circuits," *IEEE Trans. Microwave Theory Tech.*, vol. MTT-31, pp. 567–573, July 1983.

[5] C.-K. C. Tzuang and T. Itoh, "High-speed pulse transmission along a slow-wave CPW for monolithic microwave integrated circuits," *IEEE Trans. Microwave Theory Tech.*, vol. MTT-35, pp. 697–704, Aug. 1987.

[6] J. P. K. Gilb and C. A. Balanis, "Transient analysis of distortion and coupling in lossy coupled microstrips," *IEEE Trans. Microwave Theory Tech.*, vol. 38, pp. 1894–1899, Dec. 1990.

[7] D. Mirshekar-Syahkal, "An accurate determination of dielectric loss effect in monolithic microwave integrated circuits including microstrip and coupled microstrip lines," *IEEE Trans. Microwave Theory Tech.*, vol. MTT-31, pp. 950–954, Nov. 1983.

[8] T.-C. Mu, H. Ogawa, and T. Itoh, "Characteristics of multiconductor, asymmetric, slow-wave microstrip transmission lines," *IEEE Trans. Microwave Theory Tech.*, vol. MTT-34, pp. 1471–1477, Dec. 1986.

[9] T. Uwano and T. Itoh, "Spectral domain approach," in *Numerical Techniques for Microwave and Millimeter-Wave Passive Structures*, T. Itoh, Ed. New York: Wiley, 1989, ch. 5, pp. 334–380.

[10] R. H. Jansen, "The spectral-domain approach for microwave integrated circuits," *IEEE Trans. Microwave Theory Tech.*, vol. MTT-33, pp. 1043–1056, Oct. 1985.

[11] J. P. Gilb and C. A. Balanis, "Pulse distortion on multilayer coupled microstrip lines," *IEEE Trans. Microwave Theory Tech.*, vol. 37, pp. 1620–1628, Oct. 1989.

[12] M. Abramowitz and I. A. Stegun, *Handbook of Mathematical Functions*. New York: Dover, 1972.

[13] A. R. Von Hippel, *Dielectrics and Waves*. New York: Wiley, 1954.

[14] S. Ramo, J. R. Whinnery, and T. Van Duzer, *Fields and Waves in Communication Electronics*. New York: Wiley, 2nd ed., 1984.

[15] C. A. Balanis, *Advanced Engineering Electromagnetics*. New York: Wiley, 1989.

James P. K. Gilb (S'83) was born in Phoenix, AZ on March 15, 1965. He received the bachelor of science degree in electrical engineering in 1987 from Arizona State University, graduating Magna Cum Laude. In 1989, he received the master of science degree in electrical engineering from the same institution and was chosen Outstanding Graduate of the Graduate College. He is currently pursuing a Ph.D. degree in electrical engineering at Arizona State University.

His interests include full-wave solutions of discontinuities and losses in multi-layer planar waveguide structures and transient analysis of high-speed, multi-layer digital interconnects.

Mr. Gilb is a member of Sigma Xi, Tau Beta Pi, and Eta Kappa Nu.

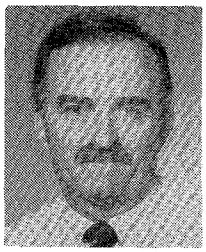

Constantine A. Balanis (S'62–M'68–SM'74–F'86) was born in Trikala, Greece. He received the BSEE degree from Virginia Tech, Blacksburg, VA, in 1964, the MEE degree from the University of Virginia, Charlottesville, VA, in 1966, and the Ph.D. degree in Electrical Engineering from Ohio State University, Columbus, OH, in 1969.

From 1964–1970 he was with NASA Langley Research Center, Hampton, VA, and from 1970–1983 he was with the Department of Electrical Engineering, West Virginia University, Morgantown, WV. Since 1983 he has been with the Department of Electrical Engineering, Arizona State University, Tempe, AZ, where he is now Regents' Professor and Director of the Telecommunications Research Center. His research interests are in low- and high-frequency antenna and scattering methods, transient analysis and coupling of high-speed high-density integrated circuits, and multipath propagation. He received the 1992 Special Professionalism Award from the IEEE Phoenix Section, the 1989 IEEE Region 6 Individual Achievement Award, and the 1987–1988 Graduate Teaching Excellence Award, School of Engineering, Arizona State University.

Dr. Balanis is a Fellow of the IEEE and a member of ASEE, Sigma Xi, Electromagnetics Academy, Tau Beta Pi, Eta Kappa Nu, and Phi Kappa Phi. He has served as Associate Editor of the IEEE Transactions on Antennas and Propagation (1974–1977) and the IEEE Transactions on Geoscience and Remote Sensing (1981–1984), as Editor of the *Newsletter* for the IEEE Geoscience and Remote Sensing Society (1982–1983), as Second Vice-President of the IEEE Geoscience and Remote Sensing Society (1984), and as Chairman of the Distinguished Lecturer Program of the IEEE Antennas and Propagation Society (1988–1991). He is the author of *Antenna Theory: Analysis and Design* (Wiley, 1982) and *Advanced Engineering Electromagnetics* (Wiley, 1989).